9-2022

Revisiting ^{228}Th as a Tool for Determining Sedimentation and Mass Accumulation Rates

Joseph J. Tamborski
Old Dominion University, jtambors@odu.edu

Pinghe Cai

Meagan Eagle

Paul Henderson

Matthew A. Charette

Original Publication Citation

Tamborski, J. J., Cai, P., Eagle, M., Henderson, P., & Charette, M. A. (2022). Revisiting ^{228}Th as a tool for determining sedimentation and mass accumulation rates. *Chemical Geology*, *607*, Article 121006. https://doi.org/10.1016/j.chemgeo.2022.121006

Chemical Geology 607 (2022) 121006

Contents lists available at ScienceDirect

Chemical Geology

journal homepage: www.elsevier.com/locate/chemgeo

Revisiting ^{228}Th as a tool for determining sedimentation and mass accumulation rates

Joseph J. Tamborski [a,b,*], Pinghe Cai [c], Meagan Eagle [d], Paul Henderson [b], Matthew A. Charette [b]

[a] Department of Ocean and Earth Sciences, Old Dominion University, Norfolk, VA, USA
[b] Department of Marine Chemistry and Geochemistry, Woods Hole Oceanographic Institution, Woods Hole, MA, USA
[c] State Key Laboratory of Marine Environmental Science, Xiamen University, Xiamen, China
[d] U.S. Geological Survey, Woods Hole Coastal and Marine Science Center, Woods Hole, MA, USA

ARTICLE INFO

Editor: Dr. Don Porcelli

Keywords:
Sedimentation
Mass accumulation
Thorium isotopes
Lead-210
Wetlands
Sea level rise

ABSTRACT

The use of ^{228}Th has seen limited application for determining sedimentation and mass accumulation rates in coastal and marine environments. Recent analytical advances have enabled rapid, precise measurements of particle-bound ^{228}Th using a radium delayed coincidence counting system (RaDeCC). Herein we review the ^{228}Th cycle in the marine environment and revisit the historical use of ^{228}Th as a tracer for determining sediment vertical accretion and mass accumulation rates in light of new measurement techniques. Case studies comparing accumulation rates from ^{228}Th and ^{210}Pb are presented for a micro-tidal salt marsh and a marginal sea environment. ^{228}Th and ^{210}Pb have been previously measured in mangrove, deltaic, continental shelf and ocean basin environments, and a literature synthesis reveals that ^{228}Th (measured via alpha or gamma spectrometry) derived accumulation rates are generally equal to or greater than estimates derived from ^{210}Pb, reflecting different integration periods. Use of ^{228}Th is well-suited for shallow (<15 cm) cores over decadal timescales. Application is limited to relatively homogenous sediment profiles with minor variations in grain size and minimal bioturbation. When appropriate conditions are met, complimentary use of ^{228}Th and ^{210}Pb can demonstrate that the upper layers of a core are undisturbed and can improve spatial coverage in mapping accumulation rates due to the higher sample throughput for sediment ^{228}Th.

1. Introduction

Particle-reactive natural and artificial radionuclides are widely used to estimate sedimentation rates in lacustrine and marine environments (Krishnaswamy et al., 1971; Koide et al., 1972). Lead-210 (^{210}Pb; $t_{1/2}$ = 22.3 y) is among the most commonly employed geochemical tools for estimating vertical accretion and mass accumulation rates (VAR and MAR, respectively) over a timescale of 100 years (Robbins, 1978; Appleby and Oldfield, 1978; Andersen, 2017; Arias-Ortiz et al., 2018), often in combination with fallout-derived cesium-137 (^{137}Cs; $t_{1/2}$ = 30.2 y) (Andersen et al., 2011). Shortly after the introduction of ^{210}Pb, Koide et al. (1973) introduced the ^{228}Th/^{232}Th isotope pair ($t_{1/2}$ = 1.9 y and ~ 14 Gy, respectively) as a complimentary sediment dating technique. Application of ^{228}Th/^{232}Th is limited to decadal timescales and is ideal for relatively rapid depositional environments (≥ 4 mm y^{-1}). Several studies have utilized ^{228}Th across a range of environmental and geomorphic conditions, including use in deep ocean basins (Koide et al., 1973; Bruland et al., 1981), along the continental slope (Chung and Chang, 1996), within coastal embayments (Hancock and Hunter, 1999), deltas (Yeager et al., 2006; Xu et al., 2015) and mangrove forests (Alongi et al., 2005).

Covering decadal timescales, ^{228}Th is well-suited to fill in relative time gaps covered by short-lived ^{234}Th ($t_{1/2}$ = 24 d) and ^{7}Be ($t_{1/2}$ = 54 d), and longer-lived ^{137}Cs and ^{210}Pb. Thus, ^{228}Th is an ideal tracer to capture modern accumulation, as compared to ^{210}Pb, and may be used to target changing sedimentation rates in response to a new boundary condition (e.g., dam removal, deforestation, and increase in storm frequency). At present ^{228}Th remains underutilized as a geochronometer, and direct comparisons between ^{210}Pb and ^{228}Th derived MARs are lacking. Considering this, the goals of this article are to (1) revisit the use of ^{228}Th as an independent tracer of sedimentation and mass accumulation rates and (2) evaluate the influence of sediment mixing on ^{210}Pb profiles using ^{228}Th as a complimentary tracer.

Measurement of excess ^{228}Th in surficial sediments provides

* Corresponding author at: Department of Ocean and Earth Sciences, Old Dominion University, Norfolk, VA, USA.
E-mail address: jtambors@odu.edu (J.J. Tamborski).

https://doi.org/10.1016/j.chemgeo.2022.121006
Received 24 January 2022; Received in revised form 7 June 2022; Accepted 26 June 2022
Available online 30 June 2022

quantitative evidence that upper sediment layers have not been disturbed during sampling, a crucial assumption in ^{210}Pb dating studies, and may be used to assess sediment mixing (Hancock and Hunter, 1999) and resuspension (Ruiz-Fernandez et al., 2001). Mixing by bioturbation and/or hydrodynamic processes can generate anomalous profiles of ^{210}Pb; sedimentation rates derived from mixed ^{210}Pb profiles will overestimate the "true" rate of accumulation (Arias-Ortiz et al., 2018). On the other hand, recent erosion will result in a lower inventory of ^{210}Pb compared to what is expected from atmospheric deposition, resulting in an underestimate of the "true" accumulation rate when using the constant rate of supply model (Appleby and Oldfield, 1978; Arias-Ortiz et al., 2018). Thus, complimentary measurement of ^{228}Th may be used to assist validation of ^{210}Pb profiles.

Whereas excess (i.e., unsupported) ^{210}Pb and ^{137}Cs are primarily derived from atmospheric sources, excess ^{228}Th is derived from aquatic and marine sources (Fig. 1). Excess ^{228}Th (^{228}Th/^{232}Th > 1) in the water column is produced by the decay of its parent ^{228}Ra ($t_{1/2}$ = 5.75 y) (Moore and Sackett, 1964; Moore, 1969). In estuarine and marine environments, dissolved ^{228}Ra may persist in the water column from sediment, riverine, and submarine groundwater sources (Swarzenski, 2007; Charette et al., 2015). Compared to radium isotopes, thorium isotopes have a much stronger affinity for particle surfaces in estuarine and marine environments (large K_D); therefore, ^{228}Th produced by the decay of ^{228}Ra (via ^{228}Ac; $t_{1/2}$ = 6.15 h) is quickly scavenged onto particle surfaces (Fig. 1) (Beck and Cochran, 2013; Santshi et al., 2006). Marine sediment ^{228}Th/^{232}Th ratios are generally near one (Turekian et al., 1996; Hancock et al., 2000). Sediment activity ratios less than one can result from the continual removal of porewater ^{228}Ra via advection (e.g., bioturbation or porewater exchange) and diffusion into the overlying water column (Carpenter et al., 1984), whereas the in-situ decay of porewater ^{228}Ra will support an authigenic ^{228}Th pool (Hancock and Hunter, 1999). In the absence of transport and advection, rapid depositional environments will have relatively high sediment ^{228}Th/^{232}Th ratios (> 1) near the sediment-water interface that decrease with depth, reflecting the 1.9 y half-life of ^{228}Th (Koide et al., 1973).

^{228}Th has received far less attention compared to ^{210}Pb as a geochemical tool for determining sedimentation and mass accumulation rates. This is likely due to analytical challenges and the complex, transient steady-state dynamics between ^{228}Th and ^{228}Ra, and with their progenitor ^{232}Th. Traditional measurements of sediment ^{228}Th involved hot-acid leaches followed by plating and subsequent measurement by alpha spectroscopy (Koide et al., 1972). Key disadvantages of this approach include entanglement of particle-bound (i.e., "detrital") and mineral lattice ^{228}Th, and long processing times. Measurement delay (generally months after sample collection) further introduces uncertainty in determining particle-bound ^{228}Th decay and ingrowth from ^{228}Ra (Koide et al., 1973). High purity germanium detectors led to improvements in bulk sediment counting for ^{228}Th, via the ^{212}Pb (238 keV) photopeak (Chen and Huh, 1999). A key advantage of gamma counting is that sediment samples can be analyzed with minimal preparation (i.e.,

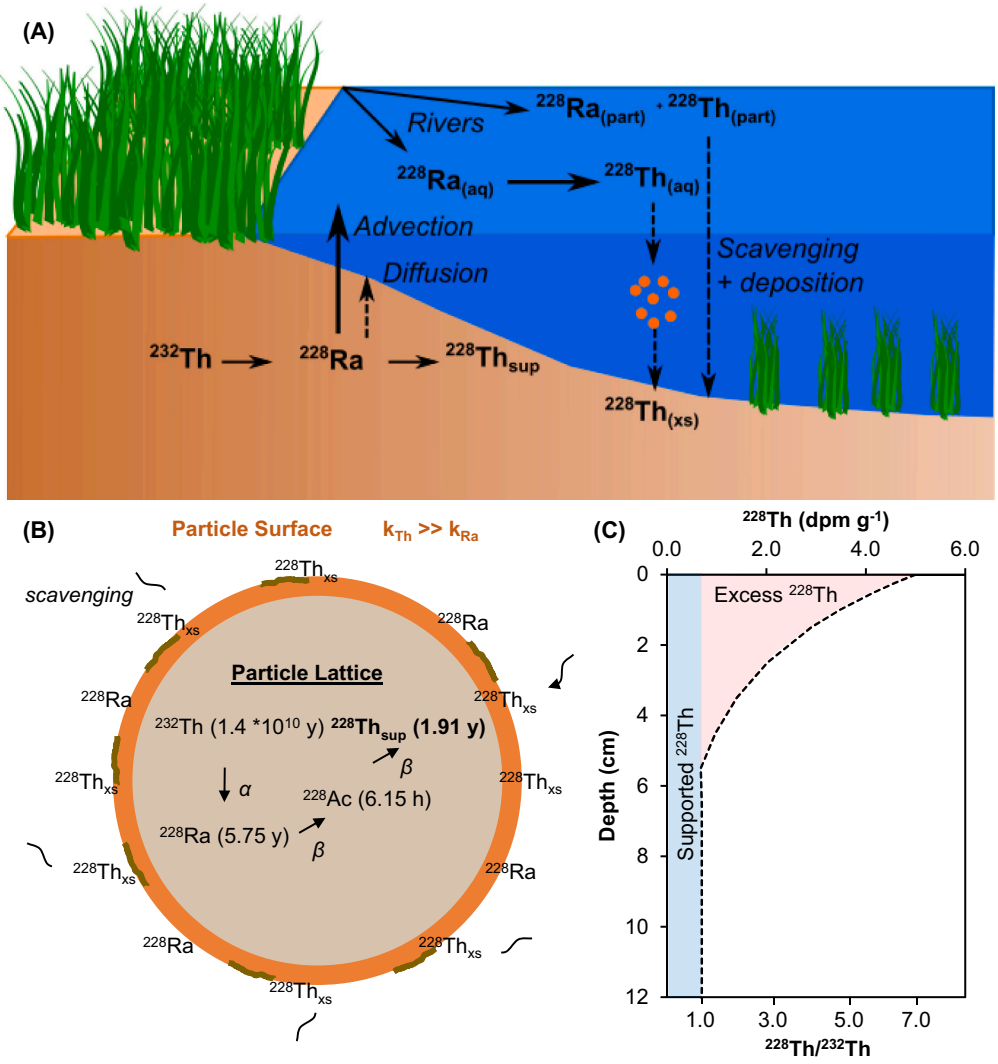

Fig. 1. Conceptual model of the ^{228}Th cycle in the marine environment (**A**), with idealized ^{228}Th distributions in particles (**B**) and activity profile/ratio in marine sediments (**C**). (part) = particulate; (aq) = aqueous; (sup) = supported activity; (xs) = excess activity. "Particle surface" (orange shading) in (**B**) encompasses the effective alpha recoil zone and the particle-bound ^{228}Th on grain coatings and secondary phases. In (**C**), the initial ^{228}Th$_{xs}$ activity of 5.0 dpm g^{-1} decreases to the supported ^{228}Th (0.7 dpm g^{-1} or ^{228}Th/^{232}Th = 1), with an apparent vertical accretion rate of 10 mm y^{-1}.

no acid leaching required) and in concert with measurements of other radionuclides of interest, including ^{210}Pb and ^{137}Cs (e.g., Alongi et al., 2005). However, gamma spectrometry cannot explicitly resolve particle surface-bound and mineral lattice ^{228}Th, and processing times for a single core section may take two or more days to count, adding up to several weeks using one detector. Further, quick counting is necessary to avoid ingrowth and decay corrections between ^{228}Th and ^{228}Ra. As a result, spatial variations in sedimentation rates are rarely assessed from more than a few cores.

The Radium Delayed Coincidence Counter (RaDeCC) has been utilized to measure surface-bound ^{228}Th and surface-exchangeable ^{224}Ra in marine sediments (Sun and Torgersen, 1998; Cai et al., 2012; Tamborski et al., 2019) and particles (Maiti et al., 2015). The RaDeCC was originally developed to measure short-lived Ra isotopes in water samples preconcentrated onto MnO_2 coated acrylic fibers (Moore and Arnold, 1996), adapted after the work of Giffin et al. (1963). As recently reviewed by Diego-Feliu et al. (2020), a sealed sample is placed in a closed He-circulation loop, where the alpha decay products of adsorbed ^{223}Ra (to ^{219}Rn) and ^{224}Ra (to ^{220}Rn) are carried into a ZnS phosphor scintillation cell (i.e., Lucas cell). Alpha decay of the radon daughters within the Lucas cell generates light, which is subsequently converted into an electronic pulse from a photomultiplier tube and then routed to a delayed coincidence circuit, where ^{219}Rn and ^{220}Rn daughters are separated and rapidly counted. The counting principles of the RaDeCC for sediment and particle samples are the same as water samples and only differ in sample preparation, geometry, and efficiency determination. Detectors are calibrated for ^{228}Th using a ^{232}Th standard (in secular equilibrium with ^{228}Th and daughters) through a method of standard addition for unique sediment matrices and sample loads (Cai et al., 2012).

In this article, we revisit the application of ^{228}Th for estimating sedimentation and mass accumulation rates using the RaDeCC system. We present two case studies (a micro-tidal salt marsh and a marginal sea) where ^{228}Th has been successfully used to determine accumulation rates, as compared to independent ^{210}Pb derived estimates. We also highlight environments and conditions in which ^{228}Th should not be used as a tracer. Here we focus on coastal and marine environments; lacustrine environments (e.g., Koide et al., 1973; Wang et al., 2020) are beyond the scope of this study. The goal of this article is not to suggest that ^{228}Th be used as an alternative or superior tool to that of ^{210}Pb and ^{137}Cs dating. Rather, we aim to demonstrate the potential of ^{228}Th as a complimentary radioisotope which may help overcome inherent challenges and biases in using ^{210}Pb and ^{137}Cs alone, including the independent validation that the top of the sediment record is intact (no recent erosion or particle reworking). Furthermore, we argue that ^{228}Th has the potential to improve spatial coverage for mapping sedimentation and mass accumulation rates in coastal environments due to the higher sample throughput for sediment ^{228}Th. Herein we use the term "mass accumulation rate" (MAR) to refer to the dry mass of material (inorganic and organic) added per unit area per unit time (g cm^{-2} y^{-1}) and "vertical accretion rate" (VAR) to refer to the net total *vertical* accretion of soil and/or sediment per unit time (i.e., "sedimentation rate"; mm y^{-1}).

2. Materials and methods

2.1. Case studies

In the Bohai and Yellow Seas, sediment cores were collected using a standard box corer (30 × 30 × 60 cm) in water depths of 15–77 m during June 2016. A total of 8 sediment cores were collected, sectioned at one-cm intervals and immediately analyzed for ^{228}Th via RaDeCC following the procedure of Cai et al. (2012), and detailed below. Details on sample collection and processing, including raw data, are available in Shi et al. (2019b; Table S3).

Sediment cores were collected from a micro-tidal salt marsh (Sage Lot Pond, MA, USA) from different marsh zones (near-creek, mid-marsh and interior of marsh) using a Russian Peat Borer over multiple seasons during 2018 and 2019 (Fig. 2). Details on sampling design and measurements can be found in Tamborski et al. (2021); sediment-bound ^{228}Th data are publicly available (Tamborski, 2020). In brief, cores were sectioned at one-cm intervals in the upper five cm of the core and at two-cm intervals thereafter; in this study we only focus on the upper 15 cm of each core. In total, 9 sediment cores were collected and processed for ^{228}Th measurement via RaDeCC following the procedure of Cai et al. (2012), as outlined in Section 2.2. Two marsh cores were additionally analyzed by gamma spectrometry over this same depth range. Core sections were dried, ground, placed in polystyrene vials and sealed with epoxy for >2 weeks prior to counting. Core 12-1C was counted within 2 months of collection for ^{228}Th, and again 1.4 years after collection for ^{210}Pb; core 6-1A was counted >1 year after collection for ^{210}Pb. Samples were analyzed on a well-type HpGe detector for ^{7}Be (477 keV) ^{210}Pb (46 keV), ^{228}Th (238 keV), ^{226}Ra (352 keV), ^{228}Ra (911 keV) and ^{234}Th (63 keV) at Woods Hole Oceanographic Institution.

2.2. Th-228 measurement via RaDeCC

In the laboratory, Ra-free Milli-Q water was added to each sediment section to form a slurry within individual containers, stirred and ultrasonicated (5–10 min). Several drops of concentrated ammonium hydroxide were added to change the slurry pH to 8.0–9.0. Next, 1.0 mL of $KMnO_4$ (3.0 g L^{-1}) and 1.0 mL of $MnCl_2$ (8.0 g $MnCl_2$*4H_2O L^{-1}) were added to each slurry to form a MnO_2 precipitate, which adsorbed any dissolved ^{228}Th (and ^{224}Ra) present in the interstitial pore fluid or that would otherwise desorb from the slurry procedure. The sediment slurry was then vacuum-filtered onto a pre-weighed 142-mm 0.7 μm GFF filter, where slurries were stirred to evenly distribute particles over the entire filter area. Filtration was stopped after water droplets were no longer observed leaving the vacuum filter outlet, and sample weights were subsequently recorded. Samples should remain moist following filtration; moisture content effects are described in Cai et al. (2012). Filtration times for coarse-grained sediments are rapid (< 1 min); fine-grained sediment filtration times may exceed 30 min. Samples were placed into sediment chambers and connected to the RaDeCC gas circulation system.

Samples described from the two case studies (Shi et al., 2019b; Tamborski et al., 2021) were counted on a RaDeCC system 8–10 days after initial collection, and again one month after collection, to quantify particle-bound ^{228}Th (Cai et al., 2014, 2015); reported ^{228}Th activities represent an average of these two measurements. Repeat measurements are recommended to reduce analytical uncertainties but are not required. By counting samples within one month of collection there would be negligible decay of any excess ^{228}Th or ingrowth from ^{228}Ra. Samples counted well after one month has passed since collection would also require analysis for ^{228}Ra to correct for ^{228}Th ingrowth (Koide et al., 1973). For each RaDeCC counting session, high-purity helium was initially recirculated through the sediment chamber (~12 L min^{-1}) for one minute. During each counting session, the 220 and total channel count rates were monitored; these channels record any decay events in a 600 ms window (optimized to target ^{220}Rn decay) and all decay events, respectively. Any significant change in the 220 and total channel count rate over time (> 10% of the mean count rate) may signify considerable moisture loss. In this scenario, sample counting stopped, and the sample moisture content was adjusted to initial (post-filtration) conditions before recounting. Sample weights were recorded following the completion of each counting session and moisture content was adjusted to pre-counting conditions with Ra-free Milli-Q water. With proper calibration and sufficient counting times (~4–10 h), measurement precision of ^{228}Th was on the order of ±2–3% (> 1000 counts in the 220 channel; Cai et al., 2015). After all counting, samples were dried to determine sediment mass. Activities of ^{228}Th were corrected for ingrowth, chance coincidence counts and channel cross talk (Moore and Arnold, 1996), and uncertainties were propagated from these terms and

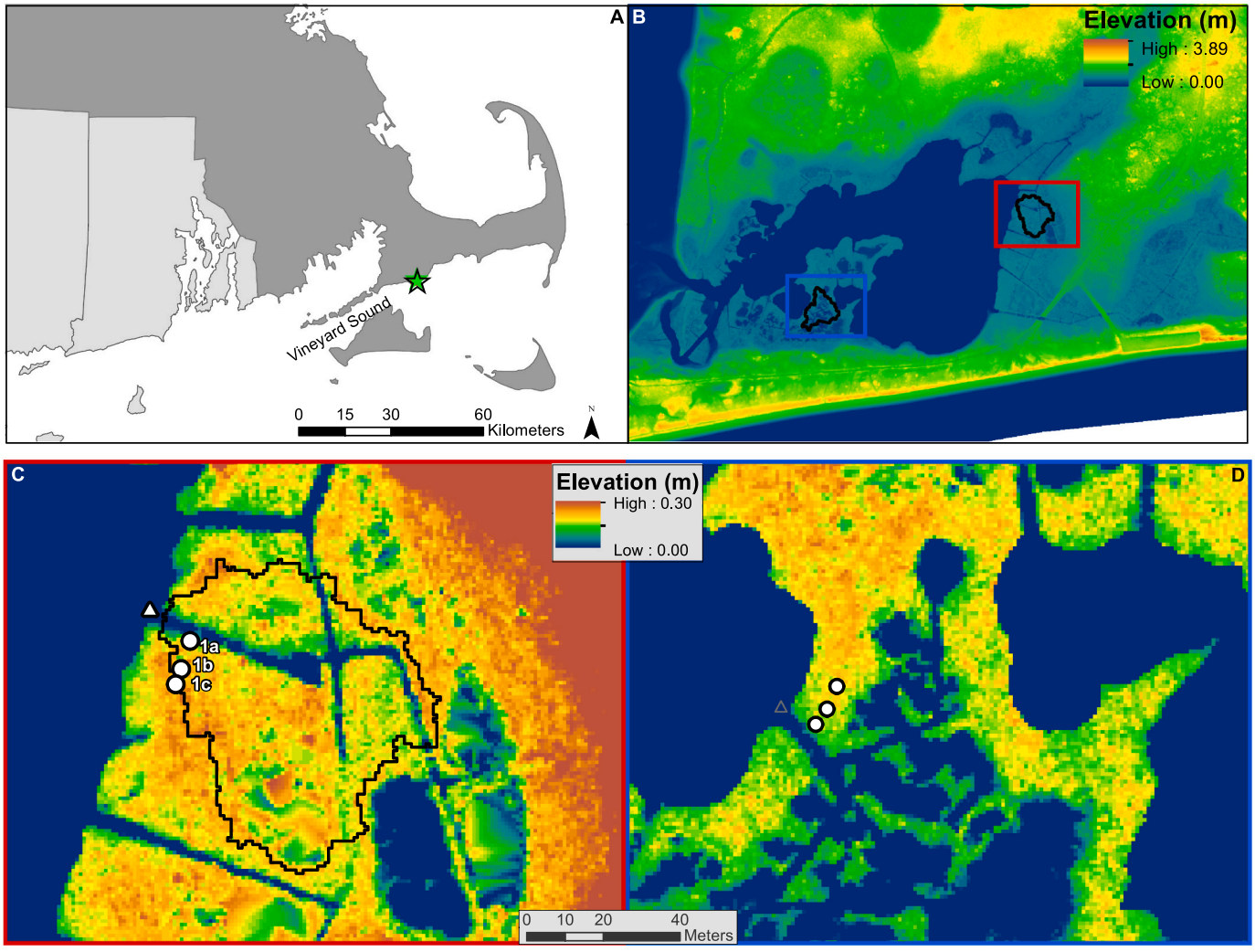

Fig. 2. Sage Lot Pond, located within the Waquoit Bay National Estuarine Research Reserve (WBNERR), Massachusetts (A,B). Sediment core sampling stations for marsh site 1 (red box; (C) and marsh site 2 (blue box; D) are depicted by white circles (a = creek; b = mid; c = interior). From Tamborski et al. (2021). (For interpretation of the references to colour in this figure legend, the reader is referred to the web version of this article.)

counting statistics, after Garcia-Solsona et al. (2008). Spreadsheets for the reduction of RaDeCC data, including ^{228}Th, are publicly available (Diego-Feliu et al., 2020).

3. Theory

In estuarine and marine environments, three different models are commonly employed for ^{210}Pb dating (Andersen, 2017); (1) the constant flux: constant sedimentation rate model (CF:CS; Krishnaswamy et al., 1971); (2) the constant initial concentration model (CIC; Robbins, 1978); and (3) the constant rate of supply model (CRS; Appleby and Oldfield, 1978). All models require the assumption of steady state, where the addition of new atoms (^{210}Pb or ^{228}Th) on the top of the sediment profile is equal to the rate of atoms decayed at depth. These models have been successfully applied to bulk ^{228}Th profiles measured via gamma spectrometry (Alongi et al., 2005; Xu et al., 2015). Arias-Ortiz et al. (2018) recently reviewed ^{210}Pb MAR models in coastal vegetated ecosystems, and the recommendations therein largely apply to models of ^{228}Th. We note that the ensuing models are based on cumulative mass depth (ρ [g cm^{-3}] × z [cm] = [g cm^{-2}]), rather than absolute depth, in order to account for any sediment compaction and downcore variation in dry bulk density (Abril, 2003; Andersen, 2017). To determine VAR (mm y^{-1}), MAR is divided by dry bulk density.

The CF:CS model (Krishnaswamy et al., 1971) assumes a constant flux of ^{228}Th and a constant mass accumulation rate,

$$^{228}Th_i = {}^{228}Th_0 \times e^{-\lambda \frac{m}{MAR}} \quad (1)$$

where $^{228}Th_i$ is excess ^{228}Th activity at depth i and ^{228}Th$_0$ is the excess ^{228}Th activity at the surface (specific activity in dpm g^{-1} or Bq g^{-1}), λ is the ^{228}Th decay constant (0.363 y^{-1}), m is the cumulative dry mass (g cm^{-2}) and MAR is the mass accumulation rate (g cm^{-2} y^{-1}). Plotting cumulative mass [X] versus ln(^{228}Th$_{xs}$) [Y] and dividing the best-fit slope by λ yields an average MAR. In contrast, the CIC model (Robbins, 1978) assumes a constant initial ^{228}Th$_0$ activity with time, such that downcore variations in ^{228}Th$_{xs}$ are directly linked to variations in MAR. Therefore, the CIC model takes the same form as Eq. (1), where time (t) is substituted for the term (m/MAR). Depth-specific ages and thus variable MARs can be determined with the CIC model; however, the CIC model is only applicable for monotonically decreasing ^{228}Th and ^{210}Pb activity profiles (Andersen, 2017; Arias-Ortiz et al., 2018).

The CRS model can be used to derive annual variations in VAR and MAR (Appleby and Oldfield, 1978) by assuming that variation in the initial specific activity at the sediment surface (^{228}Th$_0$) is linked to annual variability in VAR and MAR. For the CRS model, the total inventory of ^{228}Th$_{xs}$ within the core (I_o; dpm cm^{-2}) is calculated,

$$I_o = \sum_{i=0}^{N}([^{228}Th_i] \times \rho_i \times z_i) \quad (2)$$

where $^{228}Th_i$ is the specific activity of $^{228}Th_{xs}$ at depth i (dpm g^{-1}) to the depth of $^{228}Th_{xs}$ extinction (N), ρ_i is dry bulk density at depth i (g cm^{-3}), and z_i is the thickness of the sediment interval at depth i (cm). The inventory of $^{228}Th_{xs}$ below depth i (I_i) is determined to quantify the sediment age (t_i; y) at depth i,

$$t_i = ln\left(\frac{I_o}{I_i}\right)\lambda^{-1} \quad (3)$$

such that *VAR* and *MAR* can be estimated as the difference in sediment ages between two adjacent depth horizons over the length of core where unsupported ^{228}Th is observed. It is important to note that the sediment inventory of $^{228}Th_{xs}$ is principally sustained from the water column and pore water ^{228}Ra inventory (Fig. 1), whereas the sediment inventory of $^{210}Pb_{xs}$ is principally sustained from atmospheric deposition (Cochran et al., 1998).

When sediment mixing occurs, the use of a single radionuclide (^{210}Pb or ^{228}Th) determines an apparent sedimentation rate representative of a theoretical maximum rate (Hancock and Hunter, 1999). Following the one-dimensional advection-diffusion-decay equation (Christensen, 1982),

$$\frac{\partial A}{\partial t} = \frac{\partial}{\partial z}\left(K\frac{\partial A}{\partial z}\right) - VAR\frac{\partial A}{\partial z} - \lambda A \quad (4)$$

where the change in a given radionuclides activity (A) with time (t) can be described as a function of depth (z; cm), radioactive decay (λ; y^{-1}), the rate of sedimentation (*VAR*; cm y^{-1}) and sediment mixing (K; cm^2 y^{-1}). Taking advantage of the different half-lives of ^{228}Th and ^{210}Pb, Hancock and Hunter (1999) solve this one-dimensional equation,

$$VAR = \frac{\lambda_{Pb}/b_{Th}^2 - \lambda_{Th}/b_{Th}^2}{1/b_{Pb} - 1/b_{Th}} \quad (5)$$

$$K = \frac{\lambda_{Pb}/b_{Pb} - \lambda_{Th}/b_{Th}}{b_{Pb} - b_{Th}} \quad (6)$$

where the slope of $^{228}Th_{xs}$ versus depth is set as b_{Th} (cm^{-1}) and the slope of $^{210}Pb_{xs}$ versus depth is set as b_{Pb} (cm^{-1}), determined from log-linear plots. In this solution, ranges of *VAR* and K are determined rather than quantifying absolute uncertainties (Hancock and Hunter, 1999).

Excess, unsupported ^{228}Th activities are needed in each of these four models. $^{228}Th_{xs}$ is analogous to excess ^{210}Pb, where $^{210}Pb_{xs}$ = measured ^{210}Pb activity – ^{226}Ra activity. Samples analyzed for ^{228}Th via alpha or gamma spectrometry should be completed within several weeks of collection to limit the decay of the initial particle-bound ^{228}Th and additional ingrowth via ^{228}Ra. If alpha or gamma measurements occur several months after collection, then repeated measurements may be required to assess decay and ingrowth from $^{228}Th/^{232}Th$ activity ratios following the Bateman equations (Koide et al., 1973); however, this approach is not recommended here as it introduces additional assumptions and uncertainties. From gamma measurements within a few weeks of sample collection, $^{228}Th_{xs}$ is equal to the difference between the measured ^{228}Th and parent ^{228}Ra activities (i.e., supported ^{228}Th from the 338 or 911 keV photopeaks), under the assumption that ^{228}Ra is in secular equilibrium with ^{232}Th. If variation in grain size is minor, $^{228}Th_{xs}$ can be determined by assuming the minimum downcore ^{228}Th activity is equivalent to the supported ^{228}Th (i.e., no excess; Koide et al., 1973). This latter approach is adopted for RaDeCC measurements of ^{228}Th. It is important to note that the extinction of $^{228}Th_{xs}$ would occur within the upper ~5 to 15 cm under accretion rates ≥4 to 15 mm y^{-1}. Thus, calculating a detailed chronology based on a limited number of shallow data points from either the CRS or CIC models may not be appropriate, and the CF:CS model would be preferable (Arias-Ortiz et al., 2018). Considering this, we focus on the CF:CS model for the estimation of MAR and VAR here for the two presented case studies.

3.1. Estimation of MAR and VAR

The CF:CS model was solved in R (R Core Team, 2020) using the york function from the IsoplotR package (Vermeesch, 2018). Briefly, given uncertainties in both ^{228}Th and accumulated mass or depth (i.e., y and x), the york function finds the best fitting straight line using the least-squares algorithm of York et al. (2004). Analytical uncertainties in ^{228}Th were transformed to $ln^{228}Th$ according to:

$$ln^{228}Th_\sigma = 0.434\frac{^{228}Th_\sigma}{^{228}Th} \quad (7)$$

where $^{228}Th_\sigma$ is the analytical uncertainty for ^{228}Th (specific activity in dpm g^{-1} or Bq g^{-1}). Here we assume that the uncertainty of accumulated mass and depth is 1% and is constant through the core. Uncertainty is rarely evaluated for these terms given the difficulty in parameterization. The benefit of using the york function versus a linear least squares approach is that it discounts highly uncertain points, which are common at the base of radioisotope profiles, relative to better constrained shallower points. The code used for this analysis, as well as an example, is provided in the Supplementary Material. Where appropriate, MARs were additionally determined using ^{210}Pb data in the CRS model (Appleby and Oldfield, 1978).

4. Results and discussion

Herein we present results from the salt marsh and marginal sea case studies to demonstrate the application of ^{228}Th for estimating sedimentation and mass accumulation rates, in part validated by ^{210}Pb based approaches. To provide broader context for these two cases, we performed a literature survey of studies that have utilized both ^{210}Pb and ^{228}Th for estimating sedimentation and/or mass accumulation rates in coastal and marine environments. We also present scenarios for which ^{228}Th may not be a suitable tracer for VAR and MAR determination.

4.1. Micro-tidal salt marsh (Sage Lot Pond, USA)

Sage Lot Pond is a fringing, micro-tidal (~0.5 m) marsh site located in Cape Cod, MA, USA (Fig. 2). There is no riverine source of sediment in this protected embayment, where the dry bulk density of marsh sediments (~0.1–0.2 g cm^{-3}) is relatively constant down to the peat-sand interface. Sediment core information and near surface-bound ^{228}Th data are publicly available (Tamborski, 2020).

The RaDeCC system measures near surface-bound ^{228}Th, while gamma spectrometry measures bulk ^{228}Th (surface-bound and lattice-bound). For this peaty marsh sediment, bulk ^{228}Th at the surface of the marsh (8.21 dpm g^{-1}) decreases to lower activities (1.7–2.1 dpm g^{-1}) below 10 cm (Fig. 3). Surface-bound ^{228}Th activities measured via RaDeCC similarly decrease with depth, from a maximum of ~5 dpm g^{-1} at the marsh surface towards supported activities (0.4–0.5 dpm g^{-1}) from 8 to 14 cm. The surface-bound fraction of ^{228}Th is between 57 and 67% of the total ^{228}Th pool near the marsh surface, declining to 38–44% of the total ^{228}Th pool below 10 cm. In comparing profiles of $^{228}Th_{xs}$, there is relative agreement between RaDeCC and gamma-based approaches when measurements are conducted rapidly (Fig. 3).

Cores collected from the same marsh stations, over multiple seasons, show that surface-bound ^{228}Th distributions do not significantly vary over time below 0–1 cm (0.1 g cm^{-2}; Fig. 4a), and thus the system is in steady-state. Comparison of ln $^{228}Th_{xs}$ profiles between different marsh zones (creek, mid and interior of the marsh) suggests that apparent MARs are spatially variable (Fig. 4b), highlighting a key advantage of using the RaDeCC system for rapid assessment of MAR and VAR. From the RaDeCC measurements, the mean (± one standard deviation) MAR

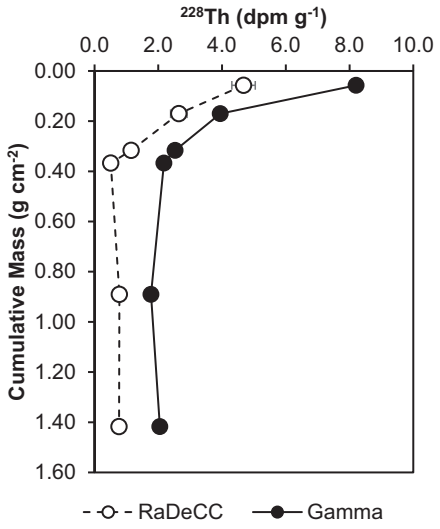

Fig. 3. Comparison between RaDeCC (near surface) and gamma (bulk) ^{228}Th activity profiles in sediments from a micro-tidal salt marsh (core 12-1C; Sage Lot Pond).

derived from the CF:CS model using the least-squares algorithm of York et al. (2004) is 0.10 ± 0.03 g cm^{-2} y^{-1} (n = 9), in agreement with MAR derived from the CRS model (0.09 ± 0.03 g cm^{-2} y^{-1}; **Fig. S1a**). This is equivalent to a VAR of 8.1 ± 2.6 mm y^{-1}. Using ^{210}Pb (CRS model; ± one standard deviation), MAR is 0.041 ± 0.025 g cm^{-2} y^{-1} for a creek marsh station (core 6-1A), or 3.0 ± 1.8 mm y^{-1}. From the CF:CS model using the York et al. (2004) algorithm, MAR is 0.022 ± 0.003 g cm^{-2} y^{-1} (cores 6-1A and 12-1C).

Sedimentation and mass accumulation rates have been independently measured at Sage Lot Pond using ^{210}Pb. A ^{210}Pb-based CRS age model was used for three cores collected in 2013 and 2014 (two low marsh cores, one high marsh core) to assess decadal variability in sedimentation rates (Gonneea et al., 2019). Mean low marsh MARs over the last decade of the ^{210}Pb record (2003–2013) range from 0.038 to 0.062 g cm^{-2} y^{-1} (Gonneea et al., 2018), somewhat lower than the ^{228}Th model estimates here (Table 1).

Here we apply the solution provided by Hancock and Hunter (1999) to evaluate the potential for sediment mixing in overestimating VAR (Eqs. (5) & (6)). We use an average of the slopes for ^{228}Th$_{xs}$ (−0.063 cm^{-1}; n = 9) and ^{210}Pb$_{xs}$ (−0.0046 cm^{-1}; n = 4) versus depth in the low marsh (Fig. 5), yielding an integrated VAR of 3.0 mm y^{-1} and a sediment mixing coefficient of 1.4 cm^2 y^{-1}. This VAR should be regarded as a lower-limit, as compared to physical measurements of VAR using surface elevation tables (3.946 mm y^{-1} from 2013 to 2018; station 2040; NOAA NERRS, 2020). Further, there was no measurable excess ^{234}Th (via gamma spectrometry) in these marsh sediments, while ^{7}Be (~7–8 dpm g^{-1}) was only observed in the top one cm of sediment (this study; Gonneea et al., 2018). Thus, it seems unlikely that sediment mixing and redistribution of ^{228}Th would lead to an overestimation of VAR for this site. Further, this lower-limit rate is comparable to the rate of relative sea level rise for this region (2.92 ± 0.17 mm y^{-1}; NOAA station 8,447,930, Woods Hole, Massachusetts). Absolute differences between MARs and VARs derived from ^{228}Th (nine cores) and ^{210}Pb (four cores) approaches may reflect differences in sampling density and spatial heterogeneity between sites, while relative differences between surface elevation table measurements and radionuclide-based approaches may be related to inherent method assumptions.

4.2. Marginal Sea (Bohai & Yellow Seas)

Sediment ^{228}Th data for the Bohai and Yellow Seas are summarized in Table S3 of Shi et al. (2019b). Particle-bound ^{228}Th activities displayed an apparent grain size effect between cores, where higher porosities (and inferred smaller grain sizes) reflect higher ^{228}Th activities; however, individual profiles did not show significant downcore variation in porosity (Fig. 6). Unsupported ^{228}Th activities were greatest at shallow depths and exponentially decreased to ~5 cm depth towards supported activities (~0.5–0.9 dpm g^{-1}), taken as the lowest measured ^{228}Th activity within each profile over an equivalent range in porosity. Mass accumulation rates derived from the CF:CS model vary from 0.35 ± 0.01 g cm^{-2} y^{-1} to 1.58 ± 0.12 g cm^{-2} y^{-1}, or VARs of 3.8 ± 0.1 mm y^{-1} to 19.4 ± 1.5 mm y^{-1}, comparable to the CRS model (**Fig. S1b**). The highest sedimentation rates are found near major river deltas and close to the coast (Fig. 6c). Independent estimates of ^{210}Pb-derived VAR display similar spatial patterns and are generally lowest in sandy areas (< 3.0 mm y^{-1}), higher in mud areas (1.5–24.3 mm y^{-1} with a mean of 5.9 mm y^{-1}) and highest near major river deltas (>20 mm y^{-1} with maximum sedimentation rates of 96 mm y^{-1}) (Qiao et al., 2017).

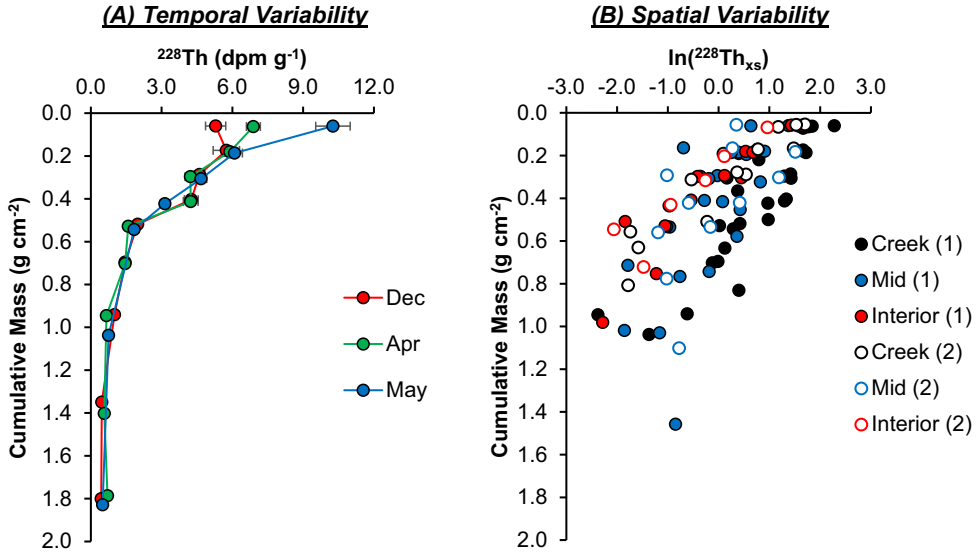

Fig. 4. Seasonal ^{228}Th profiles in sediments from a micro-tidal salt marsh (Sage Lot Pond station *creek-1*; **A**) and composite *ln* excess ^{228}Th profiles across different marsh zones and creeksheds (**B**).

Table 1
Summary of sedimentation and mass accumulation rates derived from ^{228}Th and ^{210}Pb based models. Only studies where both isotopes were used are listed.

Location	Environment	^{228}Th	^{210}Pb	Reference
Vertical accretion rates (mm y^{-1})				
Baja California	Ocean basin	8.8	3.5	Koide et al. (1973)
northern Taiwan	Continental slope	2.5–4.2	2.5–5.2	Chung and Chang (1996)[a]
Port Phillip Bay, Australia	Embayment	14.0 ± 1.3	4.1 ± 0.2	Hancock and Hunter (1999)[b]
Changjiang LDE	River delta estuary	45	12	Xu et al. (2015)[c]
Mass accumulation rates (g cm^{-2} y^{-1})				
Santa Barbara Basin	Ocean basin	0.096	0.092	Bruland et al. (1981)
Santa Monica Basin	Ocean basin	0.033–0.035	0.020	Huh et al. (1987)
Jiulongjiang Estuary	Mangrove forest	3.84 ± 0.72	7.5 ± 3.0	Alongi et al. (2005)[d]
Sage Lot Pond, MA	Salt marsh	0.048 ± 0.002	0.022 ± 0.003	This study; core 12-1C
Sage Lot Pond, MA	Salt marsh	0.10 ± 0.03	0.038–0.062	This study; Gonneea et al. (2018)[e]

[a] Rate inferred based on depth of ^{228}Th$_{xs}$ extinction.
[b] Apparent (maximum) rates of layer 2. Note that solving for *S* (and *K*) using ^{228}Th and ^{210}Pb together yields *VAR* between 0 and 1.5 mm y^{-1} and *K* of 5.0 ± 1.0 cm^2 y^{-1}
[c] ^{228}Th from CIC model, 11 to 20 cm depth, core B7
[d] Core 3564, mixed layer <2 cm depth, ^{228}Th profile MAR from Arias-Ortiz et al. (2018)
[e] Averages of RaDeCC estimates for ^{228}Th (n = 9); range of ^{210}Pb-gamma low marsh cores using the CRS model.

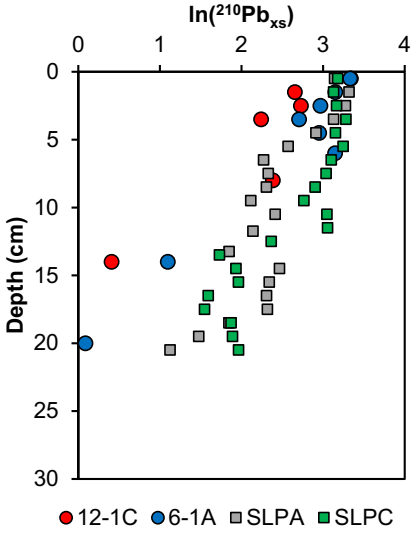

Fig. 5. Profiles of ^{210}Pb$_{xs}$ vs depth used in the simultaneous sedimentation and mixing model for the micro-tidal marsh site Sage Lot Pond, including cores from this study (12-1C and 6-1A) and previously collected low marsh cores (SLPA and SLPC; Gonneea et al., 2018).

4.3. Literature synthesis

Several studies have used ^{228}Th and ^{210}Pb concurrently to estimate sedimentation and mass accumulation rates, in addition to the two case studies highlighted here (Table 1; Fig. 7). MAR and VAR determined from ^{228}Th tends to exceed estimates derived from ^{210}Pb; this is likely a function of their integration periods. The half-life of ^{210}Pb is approximately ten times longer than ^{228}Th and as a result, ^{210}Pb integrates over a longer time period (~100 y) compared to ^{228}Th (~10 y). A recent (annual to decadal) increase in sedimentation would bias estimates derived from ^{228}Th towards higher rates in comparison to ^{210}Pb; this hypothesis requires further testing of ^{228}Th and ^{210}Pb at sites of known changes in sedimentation rates. With this said, Alongi et al. (2005) reported MAR derived from ^{210}Pb that was a factor of two greater than MAR derived from ^{228}Th (Jiulongjiang Estuary). Thus, a more robust comparison between these two isotopes across a range of environmental and geomorphic conditions is warranted. If sediment mixing occurs, then MAR and VAR estimated from both ^{228}Th and ^{210}Pb approaches would be overestimated, as the ^{210}Pb distribution should be equally affected by sediment mixing over equivalent depths.

4.4. Sensitivity analysis

An example of the CF:CS model based on the least-squares algorithm of York et al. (2004) is presented in Fig. 8. The deepest section of core H11 (Yellow Sea) approaches the supported ^{228}Th activity (0.94 dpm g^{-1}). The combined analytical uncertainties of the measured ^{228}Th and the supported ^{228}Th activity results in an excess of 0.05 ± 0.06 dpm g^{-1} just above the supported ^{228}Th sediment horizon; this highly uncertain point receives a lower ranking in the determination of the linear least-squares regression. The advantage to this approach is that it partially removes any subjective error and bias in assigning a cut-off value for what may be considered an excess ^{228}Th value. In this approach, VAR is 8.44 ± 0.20 mm y^{-1}. If VAR were calculated from a traditional linear least-squares regression without taking into account the analytical uncertainty of the individual measurements, VAR would equal 6.23 ± 0.56 mm y^{-1}, a difference of 37%. If the deepest core section was not used in the linear regression, VAR would increase to 7.65 ± 0.64 mm y^{-1}, a difference of 23% from excluding a single point. This highlights the robustness of using the least-squares algorithm of York et al. (2004) with the CF:CS model for both ^{228}Th and ^{210}Pb-based applications.

The CF:CS model developed based on the least-squares algorithm of York et al. (2004) was applied to select published datasets that reported individual measurement uncertainties. Mass accumulation in a mangrove forest environment (core no. 3564; Alongi et al., 2005), and as reviewed by Arias-Ortiz et al. (2018), was previously determined to equal 3.84 ± 0.72 g cm^{-2} y^{-1} using ^{228}Th (Table 1); MAR derived from the modified CF:CS model used here is equivalent to 4.05 ± 0.24 g cm^{-2} y^{-1}. Similarly, ^{210}Pb derived MAR (core no. 3562; checked by ^{137}Cs) was reported as 1.95 ± 0.40 g cm^{-2} y^{-1}; ^{210}Pb MAR derived from the modified CF:CS model is 2.10 ± 0.06 g cm^{-2} y^{-1}. The difference between the previously reported MAR's and the values estimated here can be attributed to the way that individual measurement uncertainties for both ^{228}Th and ^{210}Pb are weighted in the least-squares algorithm of York et al. (2004). By considering individual measurement uncertainties, the MAR relative uncertainty is substantially reduced.

The choice of the supported ^{228}Th activity from RaDeCC measurements is critical for accurate estimation of MAR and VAR. Consider the above example, core H11 from the Yellow Sea. The supported ^{228}Th activity was chosen as the lowest value within the profile. A 25% variation in the supported ^{228}Th activity (0.71–1.18 dpm g^{-1}) would result in a minimum and maximum VAR of 7.7 ± 0.3 mm y^{-1} and 10.3 ± 0.2 mm y^{-1}, respectively. Thus, the choice of the supported activity can introduce considerable uncertainty in estimating MAR and VAR and should therefore be chosen with caution. A key assumption is that the supported ^{228}Th measured downcore is representative of present-day supported ^{228}Th activities. This assumption would be violated only if the sediment deposited in the past is compositionally distinct from recently deposited sediment (e.g., derived from a new source; change in the median grain size and mineralogy). Uncertainty in the supported ^{228}Th activity can potentially be reduced by collecting and analyzing

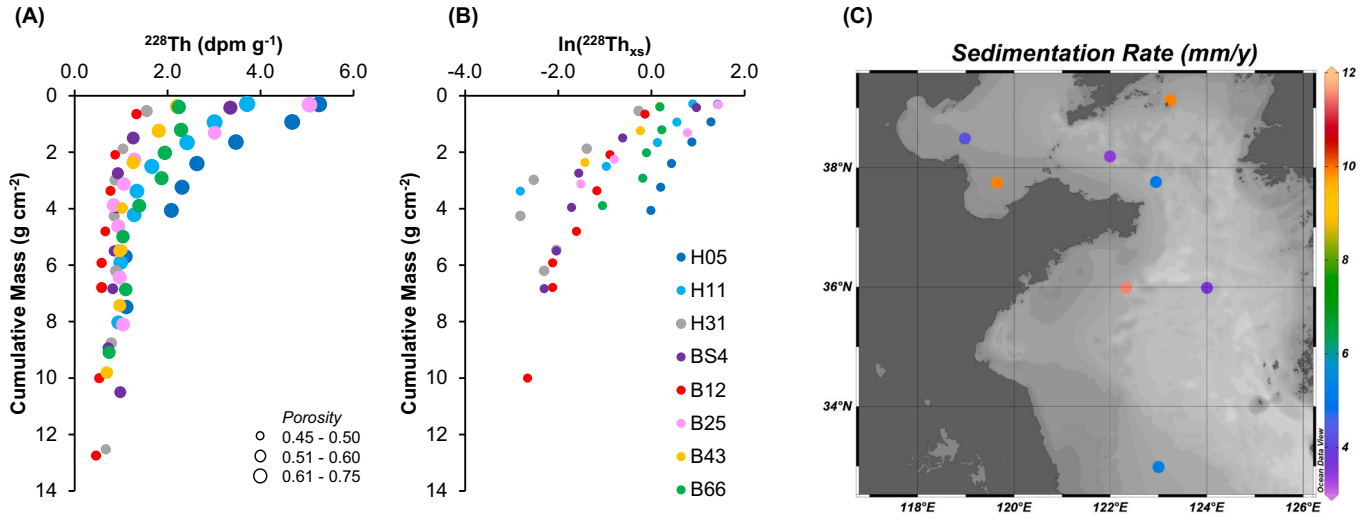

Fig. 6. ^{228}Th profiles in sediments from a marginal sea (Bohai and Yellow Seas, China), with point-size scaled as a function of porosity (**A**) and ln ^{228}Th$_{xs}$ profiles (**B**), including the spatial distribution of VAR (**C**). Data are adopted from Shi et al. (2019b). Supported ^{228}Th activities were taken as the lowest measured activity at depth within each core (~0.5–0.7 dpm g^{-1}). (For interpretation of the references to colour in this figure legend, the reader is referred to the web version of this article.)

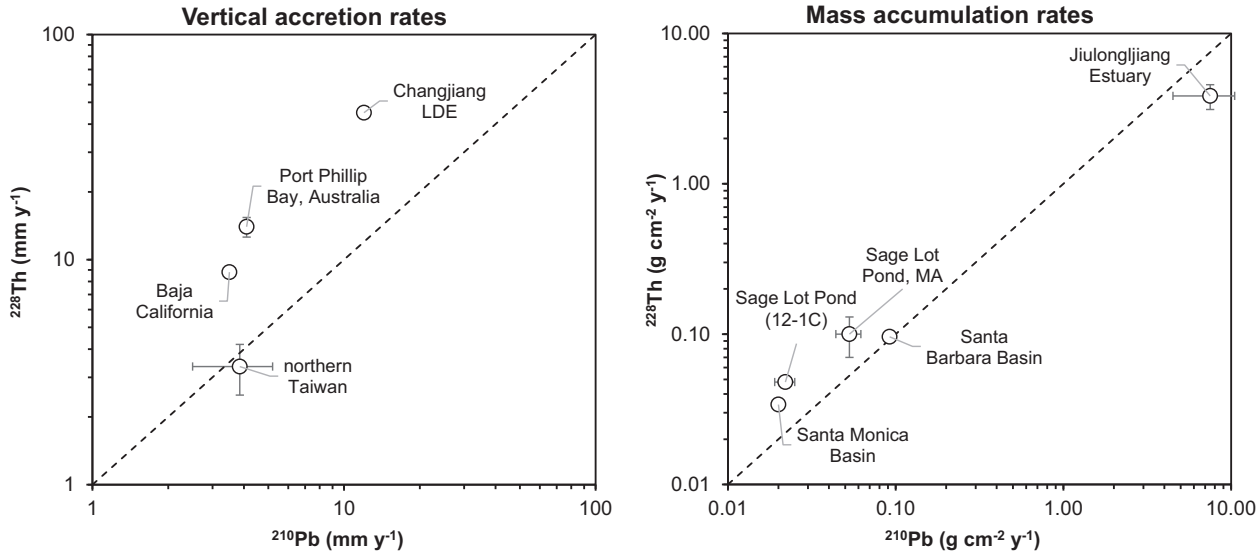

Fig. 7. Comparison between VAR and MAR derived from ^{228}Th and ^{210}Pb based models. Data are summarized in Table 1.

multiple cores from a given region (e.g., Fig. 4a).

4.5. Assumptions

The following must be considered to ensure proper utilization of ^{228}Th as a tool for calculating VAR and MAR: (1) steady-state; (2) grain size variation; and (3) redistribution of ^{228}Th following deposition.

4.5.1. Steady-state

Steady-state must be assumed depending on the accumulation model used. Given the high particle-water partition coefficient (K_d) for Th in seawater on inorganic and organic substrates (Santschi et al., 2006), we assume uniform scavenging removal of ^{228}Th, although we acknowledge that "particle concentration effects" (Honeyman et al., 1988) require further study in this application. In the case of the CF:CS model, the steady-state assumption includes both a constant input of ^{228}Th from the water column to the sediments (i.e., constant scavenging) and a constant MAR over the integration period of the core (previous decade). This assumption may be violated in environments impacted by submarine groundwater discharge, with seasonally or annually variable water column ^{228}Ra inventories, or in environments prone to sporadic inputs of dissolved ^{228}Ra, for example near an ephemeral stream or river. If MARs are expected to vary over the last several years, for example in response to a hurricane, then the steady-state assumption may also be violated; however, the CRS model may be used if the rate of ^{228}Th supply does not vary over time. When possible, duplicate sediment cores should be collected from different time periods to test the assumptions of the chosen MAR model (e.g., Fig. 4a).

4.5.2. Grain size

Sediment grain size partly controls the distribution of ^{228}Th (Fig. 9), similar to ^{210}Pb (Andersen, 2017). Smaller grain sizes, and thus larger specific surface areas, permit both a larger effective alpha recoil-zone from the mineral lattice (^{228}Th decay to ^{224}Ra) and a larger specific surface-area for adsorption. Organic ligands can increase the sorption of Th onto particle surfaces (Santschi et al., 2006); taken together, a clay-

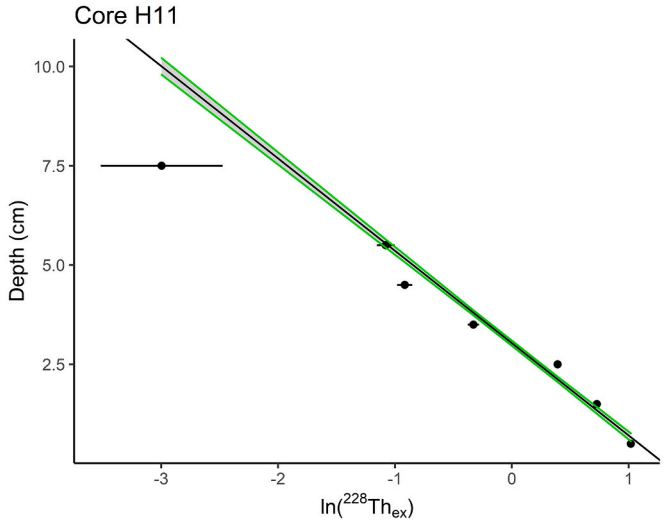

Fig. 8. An example of the CF:CS model developed based on the least-squares algorithm of York et al. (2004). Gray and green shading represents the 95% confidence-interval of the best-fit linear least-squares regression. The deepest core section at 7.5 cm depth approaches the supported ^{228}Th activity and is highly uncertain, receiving a lower weight in the linear least-squares regression. (For interpretation of the references to colour in this figure legend, the reader is referred to the web version of this article.)

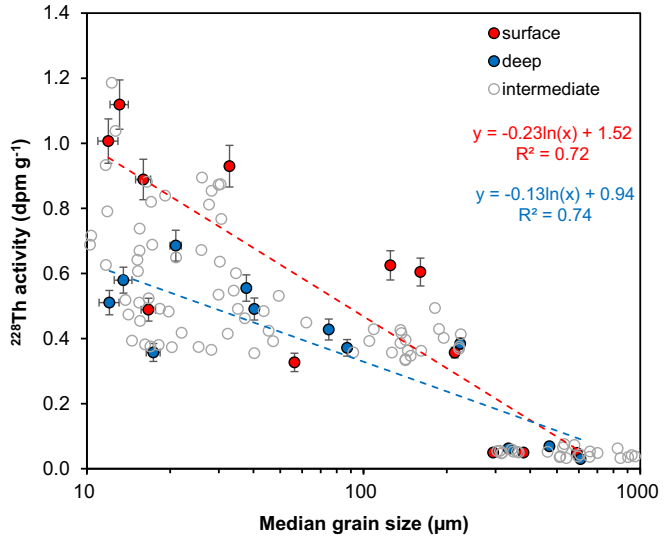

Fig. 9. Median grain size versus ^{228}Th specific activity measured via RaDeCC. Data are from the Yangtze River estuary and adjacent continental shelf (Cai et al., 2014) and a sandy beach (Weitou Bay; Cai et al., 2020). Data are classified as surface (0–1 cm), deep (deepest section of each core; 14–17 cm in Yangtze River Estuary; 29–35 cm Weitiou Bay), and intermediate (all other depth intervals).

rich sediment may have a greater abundance of Th compared to sandier sediments. The distribution of $^{228}Th_{xs}$ downcore is principally controlled by radioactive decay, and thus it is unlikely measured ^{228}Th activity and grain size will vary linearly for a single core. This concept is illustrated in Fig. 9, where surface (0–1 cm) ^{228}Th activities generally exceed deep ^{228}Th activities over equivalent ranges in grain size for an estuarine-shelf transition zone (Cai et al., 2014) and a sandy beach system (Cai et al., 2020). Similar to ^{210}Pb, coring sites should be chosen that have minor variations in sediment texture and minerology (Andersen, 2017).

Determination of supported ^{228}Th from RaDeCC measurements is only possible when downcore variations in grain size are minor. This should be determined on a per core basis, including any abrupt change in the median grain size (e.g., 10%) and shift in the cumulative grain size distribution (e.g., incorporation of more fines). An example of grain size variation in controlling ^{228}Th activity is shown in Fig. 6a. In this marginal sea environment, higher porosities (e.g., cores B25, H05) correspond to higher activities of ^{228}Th. While bulk grain size (inferred from porosity) varies substantially between these various cores, bulk grain size does not significantly vary downcore, and thus supported ^{228}Th can be determined to estimate MARs from each of these cores. Downcore variation in grain size, for example in a layered marsh environment (mud layer overlying sand), illustrate changes in ^{228}Th activity that would violate this assumption (e.g., Shi et al., 2019a). In the high energy Yangtze River estuary, sediment cores show downcore variations in grain size (Table 1 of Cai et al., 2014) and are significantly bioturbated, based on profiles of excess ^{234}Th. As a consequence, ^{228}Th profiles are constant with depth, and in some cases have the highest ^{228}Th activities at mid and bottom depth horizons, such that ^{228}Th cannot be used for determining VAR or MAR. It is critically important that this assumption is met for RaDeCC measurements in order to avoid misinterpretation of ^{228}Th depth variability due to changes in mass accumulation and sedimentation. This assumption is less critical when ^{228}Th is rapidly measured by gamma spectrometry, as the supported ^{228}Th can be directly measured via ^{228}Ra.

4.5.3. *Sediment mixing and redistribution of ^{228}Th following deposition*

The final assumption is that ^{228}Th is not redistributed following deposition. Post depositional mobility of thorium is generally insignificant (Bonatti et al., 1971; Cochran et al., 1986); thus, ^{228}Th may be a preferred tracer in rapid-depositional sedimentary environments where redistribution of ^{210}Pb and ^{137}Cs are of concern (Urban et al., 1990; Wang et al., 2020). For example, the formation of pyrite (FeS_2) can remove Pb through adsorption and inclusion within the mineral lattice, while ^{137}Cs has known subsurface mobility in organic-rich sediments (Cochran et al., 1998). A secondary concern is the efflux of the more soluble (grand)parent ^{228}Ra out of the sediments, for example via porewater exchange, bioirrigation and/or molecular diffusion (Cochran, 1979; Huh et al., 1987; Turekian et al., 1996). In Puget Sound, the efflux of dissolved ^{228}Ra was invoked as a mechanism to explain sediment ^{228}Th/^{232}Th activity ratios <1, and thus the inability of the ^{228}Th/^{232}Th isotope pair to be used in determining accumulation rates (Carpenter et al., 1984). This concern can potentially be overcome by measurement of the shallow sediment and porewater ^{228}Ra distribution from solid-phase ^{228}Ra/^{232}Th disequilibrium (Cochran, 1979; Turekian et al., 1996).

Waves, currents, bioturbation and bioirrigation can rework the sediment structure and thus redistribute ^{228}Th in the sediments (Hancock and Hunter, 1999). Substantial bioturbation can result in a "well-mixed" layer of nearly constant ^{228}Th (and ^{210}Pb) activity. In this scenario, determination of accumulation rates may be restricted to sediments below the disturbed depth horizon. Complimentary use of ^{7}Be ($t_{1/2} = 53$ d) and ^{234}Th ($t_{1/2} = 24$ d) can be used to assess the role of particle reworking by benthic fauna (Cai et al., 2014, 2015), in addition to *X*-radiographs or CT-scans. The role of bioturbation and bioirrigation must be addressed on a site-specific basis to determine whether ^{228}Th and ^{210}Pb are viable tools for estimating MARs. It is recommended that, when possible, future studies utilizing ^{228}Th analyze at least a single core for ^{210}Pb to assess the relative significance of sediment mixing (Hancock and Hunter, 1999).

5. Conclusions

Sedimentation and mass accumulation rates are not conventionally estimated using ^{228}Th, despite a favorable half-life (1.9 y) for tracing relatively rapid deposition over decadal timescales. The ^{228}Th technique falls victim to several pitfalls that additionally plague ^{210}Pb-based approaches, including grain size variations and the influence of

bioturbation. Measurement of ^{228}Th using the RaDeCC system is not a fundamentally new approach; however, several practical applications will likely emerge with implementation of ^{228}Th as a complimentary tool for estimating MARs and VARs. A single sediment sample for gamma measurement (^{228}Th, ^{210}Pb or ^{137}Cs) generally takes 1–2 days to complete. Thus, for a single core, processing times may take several weeks where only one gamma detector is available. In contrast, several cores can be analyzed for ^{228}Th via RaDeCC in just a few days from conventional four detector setups. As a result, additional sediment cores can be quickly and efficiently processed in a timely fashion and may help resolve otherwise unknown spatial patterns in MAR. Improving spatial coverage may help improve estimates of carbon accumulation in "blue carbon" habitats (Arias-Ortiz et al., 2018), as well as trace metal and nutrient accumulation within sediments. In coastal wetlands, improved spatial coverage may help to elucidate how these sensitive environments respond to sea level rise (Cochran et al., 1998). Finally, measurement of ^{228}Th can be used to quantify the degree of disturbance in shallow sediment core sections and be used concurrently with ^{210}Pb to assess rates of sediment mixing (Hancock and Hunter, 1999).

Data availability

Datasets related to this article can be found at: https://www.hydroshare.org/resource/f73a4683bf3f45d5a4cb523578ab639d/, hosted by HydroShare (Sage Lot Pond ^{228}Th core data); at: doi:https://doi.org/10.5066/F7H41QPP, hosted by www.ScienceBase.gov (Sage Lot Pond ^{210}Pb core data); and at: doi:https://doi.org/10.1016/j.gca.2019.06.026 (Table S3; Bohai and Yellow Sea ^{228}Th core data). The R code that solves the CF:CS model using the york function from the IsoplotR package is available in the supplementary material.

Declaration of Competing Interest

The authors declare that they have no known competing financial interests or personal relationships that could have appeared to influence the work reported in this paper.

Acknowledgements

This research was undertaken thanks in part to funding from the Canada First Research Excellence Fund, through the Ocean Frontier Institute. This project was supported by U.S. Geological Survey Coastal and Marine Hazards and Resources Program. Any use of trade, firm or product names is for descriptive purposes only and does not imply endorsement by the U.S. Government. PC acknowledges the support of the Natural Science Foundation of China (NSFC) through Grants No. 92058205. Thank you to Ariane Arias-Ortiz for providing previously published ^{228}Th data. We thank two anonymous reviewers, Jason Chaytor and Don Porcelli for providing comments that helped improved the manuscript.

Appendix A. Supplementary data

Supplementary data to this article can be found online at https://doi.org/10.1016/j.chemgeo.2022.121006.

References

Abril, J.M., 2003. A new theoretical treatment of compaction and the advective-diffusive processes in sediments: a reviewed basis for radiometric dating models. J. Paleolimnol. 30, 363–370. https://doi.org/10.1023/B:JOPL.0000007220.16908.d4.

Alongi, D.M., Pfitzner, J., Trott, L.A., Tirendi, F., Dixon, P., Klumpp, D.W., 2005. Rapid sediment accumulation and microbial mineralization in forests of the mangrove Kandelia candel in the Jiulongjiang Estuary, China. Estuar. Coast. Shelf Sci. 63, 605–618. https://doi.org/10.1016/j.ecss.2005.01.004.

Andersen, T.J., 2017. Some Practical Considerations Regarding the Application of 210Pb and 137Cs Dating to Estuarine Sediments. In Springer, Dordrecht, pp. 121–140.

Andersen, T.J., Svinth, S., Pejrup, M., 2011. Temporal variation of accumulation rates on a natural salt marsh in the 20th century - the impact of sea level rise and increased inundation frequency. Mar. Geol. 279, 178–187. https://doi.org/10.1016/j.margeo.2010.10.025.

Appleby, P.G., Oldfield, F., 1978. The calculation of lead-210 dates assuming a constant rate of supply of unsupported 210Pb to the sediment. Catena 5, 1–8. https://doi.org/10.1016/S0341-8162(78)80002-2.

Arias-Ortiz, A., Masqué, P., Garcia-Orellana, J., et al., 2018. Reviews and syntheses: 210Pb-derived sediment and carbon accumulation rates in vegetated coastal ecosystems - setting the record straight. Biogeosciences 15, 6791–6818. https://doi.org/10.5194/bg-15-6791-2018.

Beck, A.J., Cochran, M.A., 2013. Controls on solid-solution partitioning of radium in saturated marine sands. Mar. Chem. 156, 38–48. https://doi.org/10.1016/j.marchem.2013.01.008.

Bonatti, E., Fisher, D.E., Joensuu, O., Rydell, H.S., 1971. Postdepositional mobility of some transition elements, phosphorus, uranium and thorium in deep sea sediments. Geochim. Cosmochim. Acta 35, 189–201. https://doi.org/10.1016/0016-7037(71)90057-3.

Bruland, K.W., Franks, R.P., Landing, W.M., Soutar, A., 1981. Southern California inner basin sediment trap calibration. Earth Planet. Sci. Lett. 53, 400–408. https://doi.org/10.1016/0012-821X(81)90044-3.

Cai, P., Shi, X., Moore, W.S., Dai, M., 2012. Measurement of 224Ra:228Th disequilibrium in coastal sediments using a delayed coincidence counter. Mar. Chem. 138–139, 1–6. https://doi.org/10.1016/j.marchem.2012.05.004.

Cai, P., Shi, X., Moore, W.S., Peng, S., Wang, G., Dai, M., 2014. 224Ra:228Th disequilibrium in coastal sediments: Implications for solute transfer across the sediment-water interface. Geochim. Cosmochim. Acta 125, 68–84. https://doi.org/10.1016/j.gca.2013.09.029.

Cai, P., Shi, X., Hong, Q., Li, Q., Liu, L., Guo, X., Dai, M., 2015. Using 224Ra/228Th disequilibrium to quantify benthic fluxes of dissolved inorganic carbon and nutrients into the Pearl River Estuary. Geochim. Cosmochim. Acta 170, 188–203. https://doi.org/10.1016/j.gca.2015.08.015.

Cai, P., Wei, L., Geibert, W., Koehler, D., Ye, Y., Liu, W., Shi, X., 2020. Carbon and nutrient export from intertidal sand systems elucidated by 224Ra/228Th disequilibria. Geochim. Cosmochim. Acta. https://doi.org/10.1016/J.GCA.2020.02.007.

Carpenter, R., Peterson, M.L., Bennett, J.T., Somayajulu, B.L.K., 1984. Mixing and cycling of uranium, thorium and 210Pb in Puget Sound sediments. Geochim. Cosmochim. Acta 48, 1949–1963. https://doi.org/10.1016/0016-7037(84)90377-6.

Charette, M.A., Morris, P.J., Henderson, P.B., Moore, W.S., 2015. Radium isotope distributions during the US GEOTRACES North Atlantic cruises. Mar. Chem. 177, 184–195. https://doi.org/10.1016/j.marchem.2015.01.001.

Chen, H.Y., Huh, C.A., 1999. ^{232}Th-^{228}Ra-^{228}Th disequilibrium in East China Sea sediments. J. Environ. Radioact. 42, 93–100. https://doi.org/10.1016/S0265-931X(98)00030-7.

Christensen, E.R., 1982. A model for radionuclides in sediments influenced by mixing and compaction. J. Geophys. Res. 87 (C1), 566–572. https://doi.org/10.1029/JC087iC01p00566.

Chung, Y., Chang, W.C., 1996. Uranium and thorium isotopes in marine sediments off northeastern Taiwan. Mar. Geol. 133, 89–102. https://doi.org/10.1016/0025-3227(96)00004-7.

Cochran, J.K., 1979. The Geochemistry of 226Ra and 228Ra in Marine Deposits. Yale University.

Cochran, J.K., Carey, A.E., Sholkovitz, E.R., Surprenant, L.D., 1986. The geochemistry of uranium and thorium in coastal marine sediments and sediment pore waters. Geochim. Cosmochim. Acta 50, 663–680. https://doi.org/10.1016/0016-7037(86)90344-3.

Cochran, J.K., Hirschberg, D.J., Wang, J., Dere, C., 1998. Atmospheric deposition of metals to coastal waters (Long Island Sound, New York U.S.a.): evidence from saltmarsh deposits. Estuar. Coast. Shelf Sci. 46, 503–522. https://doi.org/10.1006/ecss.1997.0299.

Diego-Feliu, M., Rodellas, V., Alorda-Kleinglass, A., et al., 2020. Guidelines and limits for the quantification of U/Th series radionuclides with the radium delayed coincidence counter (RaDeCC). J. Geophys. Res. Oceans 125 doi:10.1029/2019JC015544.

Garcia-Solsona, E., Garcia-Orellana, J., Masque, P., Dulaiova, H., 2008. Uncertainties associated with 223Ra and 224Ra measurements in water via a delayed Coincidence Counter (RaDeCC). Mar. Chem. 109 (3–4), 198–219. https://doi.org/10.1016/j.marchem.2007.11.006.

Giffin, C., Kaufman, A., Broecker, W., 1963. Delayed coincidence counter for the assay of actinon and thoron. J. Geophys. Res. 68, 1749–1757. https://doi.org/10.1029/jz068i006p01749.

Gonneea, M., O'Keefe-Suttles, J., Kroeger, K., 2018. Collection, Analysis, and Age-Dating of Sediment Cores from Salt Marshes on the South Shore of Cape Cod, Massachusetts, from 2013 through 2014. U.S. Geological Survey data release. https://doi.org/10.5066/F7H41QPP.

Gonneea, M.E., Maio, C.V., Kroeger, K.D., et al., 2019. Salt marsh ecosystem restructuring enhances elevation resilience and carbon storage during accelerating relative sea-level rise. Estuar. Coast. Shelf Sci. 217, 56–68. https://doi.org/10.1016/J.ECSS.2018.11.003.

Hancock, G.J., Hunter, J.R., 1999. Use of excess 210Pb and 228Th to estimate rates of sediment accumulation and bioturbation in Port Phillip Bay, Australia. Mar. Freshw. Res. 50, 533–545. https://doi.org/10.1071/MF98053.

Hancock, G.J., Webster, I.T., Ford, P.W., Moore, W.S., 2000. Using Ra isotopes to examine transport processes controlling benthic fluxes into a shallow estuarine lagoon. Geochim. Cosmochim. Acta 64, 3685–3699. https://doi.org/10.1016/S0016-7037(00)00469-5.

Honeyman, B.D., Balistrieri, L.S., Murray, J.W., 1988. Oceanic trace metal scavenging: the importance of particle concentration. Deep Sea Res. Part A. Oceanogr. Res. Papers 35 (2), 227–246. https://doi.org/10.1016/0198-0149(88)90038-6.

Huh, C.A., Zahnle, D.L., Small, L.F., Noshkin, V.E., 1987. Budgets and behaviors of uranium and thorium series isotopes in Santa Monica Basin sediments. Geochim. Cosmochim. Acta 51, 1743–1754. https://doi.org/10.1016/0016-7037(87)90352-8.

Koide, M., Soutar, A., Goldberg, E.D., 1972. Marine geochronology with 210Pb. Earth Planet. Sci. Lett. 14, 442–446. https://doi.org/10.1016/0012-821X(72)90146-X.

Koide, M., Bruland, K.W., Goldberg, E.D., 1973. Th-228/Th-232 and Pb-210 geochronologies in marine and lake sediments. Geochim. Cosmochim. Acta 37, 1171–1187.

Krishnaswamy, S., Lal, D., Martin, J.M., Meybeck, M., 1971. Geochronology of lake sediments. Earth Planet. Sci. Lett. 11, 407–414. https://doi.org/10.1016/0012-821X(71)90202-0.

Maiti, K., Charette, M.A., Buesseler, K.O., Zhou, K., Henderson, P., Moore, W.S., Morris, P., Kipp, L., 2015. Determination of particulate and dissolved 228Th in seawater using a delayed coincidence counter. Mar. Chem. 177, 177–202. https://doi.org/10.1016/j.marchem.2014.12.001.

Moore, W.S., 1969. Measurement of ^{228}Ra and ^{228}Th in sea water. J. Geophys. Res. 74, 694–704. https://doi.org/10.1029/JB074i002p00694.

Moore, W.S., Arnold, R., 1996. Measurement of Ra-223 and Ra-224 in coastal waters using a delayed coincidence counter. J. Geophys. Res. Oceans 101, 1321–1329. https://doi.org/10.1029/95JC03139.

Moore, W.S., Sackett, W.M., 1964. Uranium and thorium series inequilibrium in sea water. J. Geophys. Res. 69, 5401–5405. https://doi.org/10.1029/jz069i024p05401.

NOAA NERRS, 2020. NOAA National Estuarine Research Reserve System (NERRS) System-wide monitoring program. Data accessed from the NOAA NERRS Centralized Data Management Office website. http://www.nerrsdata.org/ (2020).

Qiao, S., Shi, X., Wang, G., et al., 2017. Sediment accumulation and budget in the Bohai Sea, Yellow Sea and East China Sea. Mar. Geol. 390, 270–281. https://doi.org/10.1016/j.margeo.2017.06.004.

R Core Team, 2020. R: A Language and Environment for Statistical Computing. R Foundation for Statistical Computing, Vienna, Austria. http://www.R-project.org/.

Robbins, J., 1978. Geochemical and geophysical applications of radioactive lead. In: Nriagu, J. (Ed.), The Biogeochemistry of Lead in the Environment. Elsevier., pp. 285–393

Ruiz-Fernandez, A.C., Hillaire-Marcel, C., Ghaleb, B., Paez-Osuna, F., Soto-Jimenez, M., 2001. Isotopic constraints (210Pb, 228Th) on the sedimentary dynamics of contaminated sediments from a subtropical coastal lagoon (NW Mexico). Environ. Geol. 41, 74–89. https://doi.org/10.1007/s002540100341.

Santshi, P.H., Murray, J.W., Baskaran, M., Benitez-Nelson, C.R., Guo, L.D., Hung, C.-C., Lamborg, C., Moran, S.B., Passow, U., Roy-Barman, M., 2006. Thorium speciation in seawater. Mar. Chem. 100, 250–268. https://doi.org/10.1016/j.marchem.2005.10.024.

Shi, X., Benitez-Nelson, C.R., Cai, P., He, L., Moore, W.S., 2019a. Development of a two-layer transport model in layered muddy-permeable marsh sediments using ^{224}Ra-^{228}Th disequilibria. Limnol. Oceanogr. https://doi.org/10.1002/lno.11143.

Shi, X., Wei, L., Hong, Q., Liu, L., Wang, Y., Shi, X., Ye, Y., Cai, P., 2019b. Large benthic fluxes of dissolved iron in China coastal seas revealed by 224Ra/228Th disequilibria. Geochim. Cosmochim. Acta 260, 49–61. https://doi.org/10.1016/j.gca.2019.06.026.

Sun, Y., Torgersen, T., 1998. Rapid and precise measurement method for adsorbed 224Ra on sediments. Mar. Chem. 61, 163–171.

Swarzenski, P.W., 2007. U/Th series radionuclides as coastal groundwater tracers. Chem. Rev. 107, 663–674. https://doi.org/10.1021/cr0503761.

Tamborski, J.J., 2020. Sage lot pond Ra isotope data 2018–2019. Hydroshare. https://www.hydroshare.org/resource/f73a4683bf3f45d5a4cb523578ab639d/.

Tamborski, J., van Beek, P., Rodellas, V., et al., 2019. Temporal variability of lagoon–sea water exchange and seawater circulation through a Mediterranean barrier beach. Limnol. Oceanogr. 64, 2059–2080. https://doi.org/10.1002/lno.11169.

Tamborski, J.J., Eagle, M., Kurylyk, B.L., Kroeger, K.D., Wang, Z.A., Henderson, P., Charette, M.A., 2021. Pore water exchange-driven inorganic carbon export from intertidal salt marshes. Limnol. Oceanogr. 66, 1774–1792. https://doi.org/10.1002/lno.11721.

Turekian, K.K., Tanaka, N., Turekian, V.C., Torgersen, T., Deangelo, E.C., 1996. Transfer rates of dissolved tracers through estuaries based on 228Ra: a study of Long Island Sound. Cont. Shelf Res. 16, 863–873.

Urban, N.R., Eisenreich, S.J., Grigal, D.F., Schurr, K.T., 1990. Mobility and diagenesis of Pb and ^{210}Pb in peat. Geochim. Cosmochim. Acta 54 (12), 3329–3346. https://doi.org/10.1016/0016-7037(90)90288-V.

Vermeesch, P., 2018. IsoplotR: a free and open toolbox for geochronology. Geosci. Front. 9, 1479–1493. https://doi.org/10.1016/j.gsf.2018.04.001.

Wang, Q., Sha, Z., Wang, J., Zhong, Q., Fang, P., Ma, Y., Du, J., 2020. Vertical distribution of radionuclides in Lake Qinghai, Qinghai-Tibet Plateau, and its environmental implications. Chemosphere 259, 127489. https://doi.org/10.1016/j.chemosphere.2020.127489.

Xu, B., Bianchi, T.S., Allison, M.A., et al., 2015. Using multi-radiotracer techniques to better understand sedimentary dynamics of reworked muds in the Changjiang River estuary and inner shelf of East China Sea. Mar. Geol. 370, 76–86. https://doi.org/10.1016/j.margeo.2015.10.006.

Yeager, K.M., Santschi, P.H., Schindler, K.J., Andres, M.J., Weaver, E.A., 2006. The relative importance of terrestrial versus marine sediment sources to the Nueces-Corpus Christi Estuary, Texas: an isotopic approach. Estuar. Coasts 29, 443–454.

York, D., Evensen, N.M., Lopez Martinez, M., De Basabe Delgado, J., 2004. Unified equations for the slope, intercept, and standard errors of the best straight line. Am. J. Phys. 72 (3), 367–375. https://doi.org/10.1119/1.1632486.